CORA Cork Open Research Archive
Cartlann Taighde Oscailte Chorcaí

Title	Distinct populations of inflammatory fibroblasts and myofibroblasts in pancreatic cancer
Authors	Öhlund, Daniel;Handly-Santana, Abram;Biffi, Giulia;Elyada, Ela;Almeida, Ana S.;Ponz-Sarvise, Mariano;Corbo, Vincenzo;Oni, Tobiloba E.;Hearn, Stephen A.;Lee, Eun Jung;Chio, Iok In Christine;Hwang, Chang-Il;Tiriac, Herve;Baker, Lindsey A.;Engle, Dannielle D.;Feig, Christine;Kultti, Anne;Egeblad, Mikala;Fearon, Douglas T.;Crawford, James M.;Clevers, Hans;Park, Youngkyu;Tuveson, David A.
Publication date	2017
Original Citation	Öhlund, D., Handly-Santana, A., Biffi, G., Elyada, E., Almeida, A. S., Ponz-Sarvise, M., Corbo, V., Oni, T. E., Hearn, S. A., Lee, E. J., Chio, I. I. C., Hwang, C.-I., Tiriac, H., Baker, L. A., Engle, D. D., Feig, C., Kultti, A., Egeblad, M., Fearon, D. T., Crawford, J. M., Clevers, H., Park, Y. and Tuveson, D. A. (2017) 'Distinct populations of inflammatory fibroblasts and myofibroblasts in pancreatic cancer', Journal of Experimental Medicine, 214(3), pp. 579-596. doi: 10.1084/jem.20162024
Type of publication	Article (peer-reviewed)
Link to publisher's version	http://jem.rupress.org/content/214/3/579 - 10.1084/jem.20162024
Rights	© 2017, Öhlund et al. This article is available under a Creative Commons License (Attribution 4.0 International, as described at https://creativecommons.org/licenses/by/4.0/) - https://creativecommons.org/licenses/by/4.0/
Download date	2026-10-10 14:22:24
Item downloaded from	https://hdl.handle.net/10468/6359

University College Cork, Ireland
Coláiste na hOllscoile Corcaigh

The Journal of Experimental Medicine

SUPPLEMENTAL MATERIAL

Öhlund et al., https://doi.org/10.1084/jem.20162024

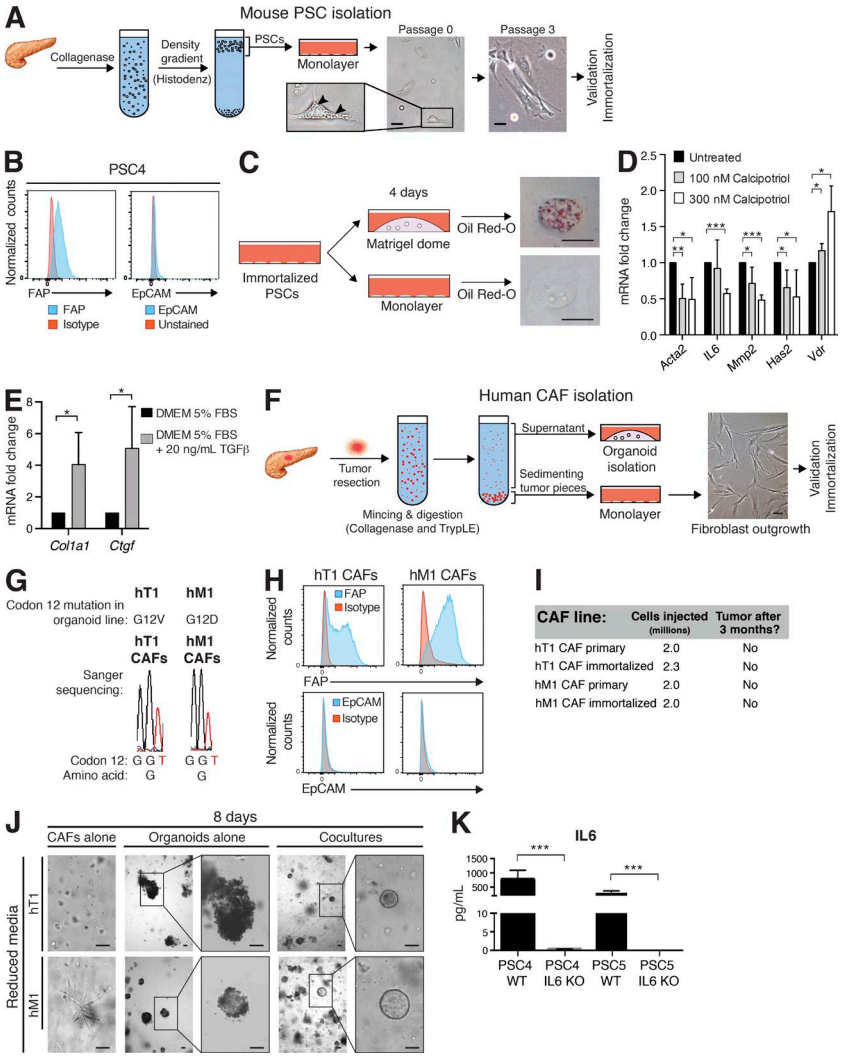

Figure S1. **Isolation and validation of mouse PSCs and human CAFs.** (A) Schematic illustration of mouse PSC isolation. After enzymatic digestion, quiescent, fat-storing PSCs were separated on a density gradient and transferred to cell culture dishes. Cell morphology and lipid droplet formation were evaluated at passage 0 and 3. Lipid droplets could still be observed in the cytoplasm at passage 0 (arrowheads), but at passage 3 the cells were fully activated and had lost all fat droplets ($n = 3$). Bars, 50 µm. (B) Representative flow histograms illustrating the expression levels of the fibroblast marker FAP and the epithelial marker EpCAM in one isolated PSC line. None of the tested PSC lines showed contamination of $EpCAM^+$ epithelial cells ($n = 3$). (C) Oil Red-O staining of immortalized PSCs cultured on plastic or embedded in Matrigel ($n = 3$). Reacquisition of lipid droplets (red stain) occurred after 4 d in Matrigel. Bars, 25 µm. (D) qPCR analysis of vitamin D analogue Calcipotriol-responsive genes in primary and immortalized PSCs cultured in monolayers and treated with 100 or 300 nM Calcipotriol for 3 d. Changes are normalized to untreated condition. As expected, *Acta2, Il6, Mmp2*, and *Has2* were down-regulated upon exposure to Calcipotriol in a dose-dependent manner, and compensatory up-regulation of the vitamin D receptor (*Vdr*) was observed. Results show mean ± SD of three biological replicates (two replicates from immortalized PSCs and one from primary PSCs). (E) qPCR analysis of TGFβ responsive genes in PSCs after 5 d of stimulation with recombinant TGFβ. Results show mean ± SD of three biological replicates. (F) Schematic illustration of the isolation of human organoids and CAFs. Bar, 100 µm. (G) Sanger sequencing results from two human tumor organoid lines compared with their patient-matched CAF lines, showing a WT *KRAS* genotype in the CAFs, which indicates no epithelial contamination in these cell lines. (H) Flow histograms of isolated human CAF lines stained for the fibroblast marker FAP and the epithelial marker EpCAM ($n = 2$). The CAF lines express FAP to a variable degree, but show no evidence of epithelial cell contamination. (I) Table summarizing the outcome after subcutaneous transplantation of primary and immortalized human CAF lines into NOD SCID gamma (NSG) mice. One mouse with two transplanted tumors (one in each flank) was performed for each CAF line. The isolated CAFs do not show evidence of transformation at 3 mo after transplantation. (J) Representative bright field images of human immortalized CAFs, human organoids, and co-cultures in reduced media conditions. Human CAFs in monoculture show various degrees of morphological activation. Organoids in monoculture do not survive in reduced media, but can be rescued in co-culture with CAFs ($n = 2$). Bars, 100 µm. (K) ELISA of IL-6 secreted from two PSC lines (PSC4 and PSC5) expressing Cas9 and short guide RNAs (sgRNAs) against IL-6, and cultured in trans-well with tumor organoids. The lines were established by combining five clones from each line to create two IL-6 knock out (KO) lines. As controls, clones with intact IL-6 expression were combined to create two IL-6 WT control lines. Results show mean ± SD of the five separate clones. *, $P < 0.05$; **, $P < 0.01$; ***, $P < 0.001$, unpaired Student's *t* test.

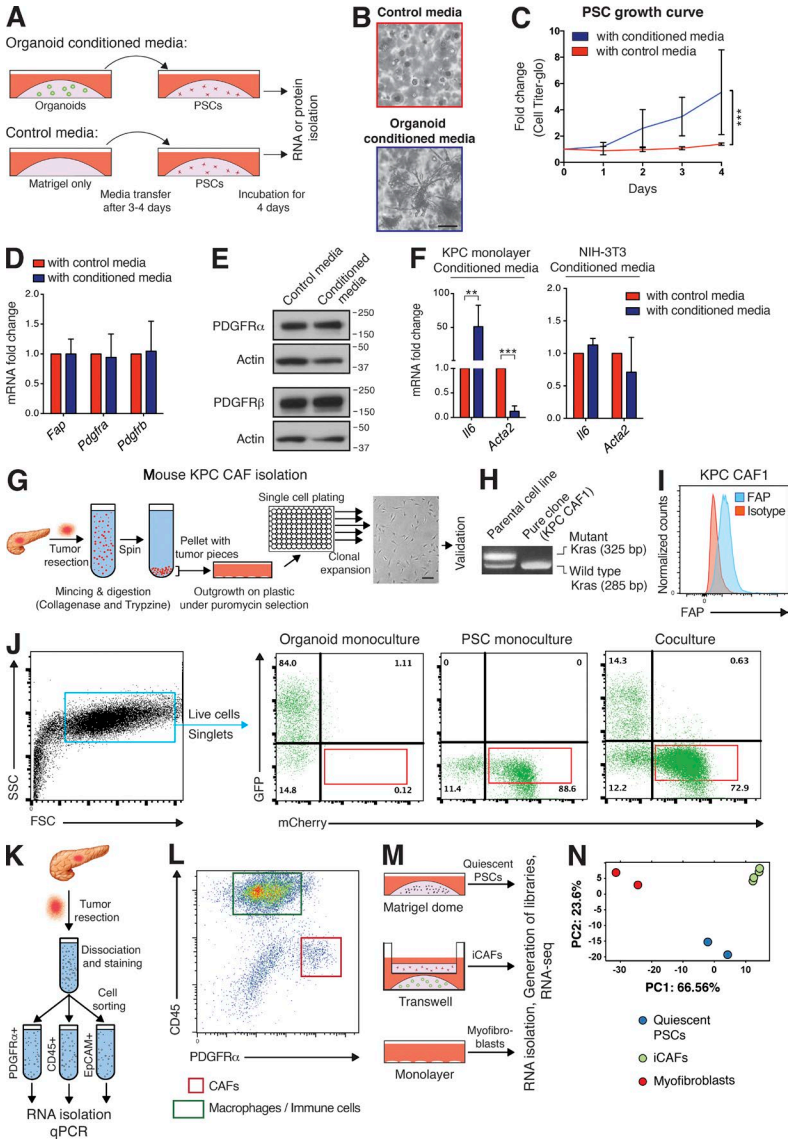

Figure S2. **Characterization of fibroblast heterogeneity in co-cultures with tumor organoids.** (A) Schematic illustration of the conditioned media experimental platform. (B) Representative bright field images of PSCs cultured with control media (Matrigel-only conditioned media) or tumor organoid–conditioned media (n = 2). Bar, 100 µm. (C) Growth curves of PSCs cultured in control media or tumor organoid conditioned media, as measured by Cell Titer-Glo. Results show mean ± SD of three biological replicates. Fold change normalized to the first time point. ***, P < 0.001, unpaired Student's t test. (D) qPCR analysis of *Fap*, *Pdgfra*, and *Pdgfrb* in PSCs cultured with control media or organoid conditioned media. Results show mean ± SD of four and three biological replicates for *Fap* and the *Pdgfr*s, respectively. No significant changes were detected, unpaired Student's t test. (E) Western blot analysis of PDGFRα and PDGFRβ in PSCs cultured with control media or tumor organoid conditioned media (n = 2). Loading control, Actin. Molecular weights in kilodaltons. (F) qPCR analysis of *Il6* and *Acta2* in PSCs cultured with control media or conditioned media from KPC tumor cells or NIH-3T3 fibroblasts in monolayer. Results show mean ± SD of two and six biological replicates for NIH-3T3 and KPC-conditioned media, respectively. **, P < 0.01; ***, P < 0.001, unpaired Student's t test. (G) Schematic illustration of KPC mouse CAF isolation. Puromycin selection was used as these cells still retain the Lox-Stop-Lox (LSL) cassette containing a puromycin resistance gene, whereas cancer cells do not as a result of cre-mediated recombination at this site. Bar, 200 µm. Two KPC CAF lines were isolated with this method (KPC CAF1 and KPC CAF2). (H) Representative example of *Kras* PCR genotyping of a KPC CAF clone and its corresponding parental CAF line, showing loss of the mutant *Kras* allele only in the clone. (I) Flow histogram of KPC CAF1 stained for the fibroblast marker FAP. Similar results were obtained for KPC CAF2. (J) Representative flow cytometric graphs showing the gating strategy for monocultures and co-cultures of mCherry-expressing PSCs and GFP-expressing organoids. Cells were gated out from debris (blue gate), and live singlets were selected. mCherry-expressing PSCs were then gated (red gate), and further analyzed for αSMA and IL-6 expression. (K) Schematic illustration of the strategy used for sorting CAFs, epithelial cells and immune cells from KPC mouse tumors. (L) Representative flow cytometric analysis of a KPC mouse tumor stained for PDGFRα$^+$ cells (CAFs) and CD45$^+$ cells (immune cells; n = 2). (M) Schematic illustration of the culture conditions of PSCs that were used to obtain the different subtypes in vitro. (N) Principal component analysis (PCA) of quiescent PSCs (n = 2), iCAFs (n = 4), and myofibroblastic PSCs (n = 2).

Table S1, provided as an Excel file, contains the RNA expression analysis (DeSEQ) and pathway analysis (GSEA) comparing quiescent PSCs, iCAFs, and myofibroblasts.